processes

MDPI

Article

Determination and Analysis of Solubility of HC-290 (Propane) in [hmim][Tf_2N]

Wei Shi, Jianrong Shi and Xiaopo Wang *

Key Laboratory of Thermo-Fluid Science and Engineering, Ministry of Education, School of Energy and Power Engineering, Xi'an Jiaotong University, Xi'an 710049, China
* Correspondence: wangxp@xjtu.edu.cn; Tel.: +86-29-82668210

Abstract: Seeking the alternative working pairs used in absorption refrigeration cycles is one of the main issues in refrigeration fields due to the drawbacks of traditional H_2O/LiBr and NH_3/H_2O, such as corrosion, crystallization, and toxicity. The imidazolium-based ionic liquid [hmim][Tf_2N] has emerged as a promising candidate as an absorbent used in absorption refrigeration systems. In addition, due to having a higher specific heat and higher latent heat of evaporation, hydrocarbons such as HC-290 have been considered as good alternative refrigerants in compression refrigeration cycles. In order to explore the possibility of using HC-290 in the absorption refrigeration cycle, the exact phase behavior of HC-290 with absorbents should be known. Therefore, in this work, the isochoric saturation method was used to determine the solubility of HC-290 in [hmim][Tf_2N] over a temperature range of 283.15 K to 343.15 K. The experimental data were modeled using the non-random two-liquid (NRTL) activity coefficient model and the Krichevsky–Kasarnovsky (K-K) fugacity model. The average absolute relative deviations for the mole fraction of HC-290 in [hmim][Tf_2N] between this work and calculated results from the models were 0.76% (NRTL) and 0.78% (K-K), and the corresponding maximum relative deviations were 3.39% and 3.24%. Based on the NRTL model, the Gibbs free energy, enthalpy change, and entropy change in the dissolution process of HC-290 in [hmim][Tf_2N] were calculated and discussed. Furthermore, the Henry's constants of various refrigerants in [hmim][Tf_2N] were calculated at 313.15 K and 333.15 K, and the results were systematically compared.

Keywords: HC-290; [hmim][Tf_2N]; solubility; NRTL model; Krichevsky–Kasarnovsky model; Henry's constant

check for updates

Academic Editor: Ali Aminian

Received: 12 February 2025
Revised: 8 March 2025
Accepted: 20 March 2025
Published: 22 March 2025

Citation: Shi, W.; Shi, J.; Wang, X. Determination and Analysis of Solubility of HC-290 (Propane) in [hmim][Tf_2N]. *Processes* **2025**, *13*, 945. https://doi.org/10.3390/pr13040945

Copyright: © 2025 by the authors. Licensee MDPI, Basel, Switzerland. This article is an open access article distributed under the terms and conditions of the Creative Commons Attribution (CC BY) license (https://creativecommons.org/licenses/by/4.0/).

1. Introduction

The absorption refrigeration cycle (ARC) can be driven by low-grade energy, such as industrial waste heat, solar energy, and other forms of residual heat [1,2]. The performance of the ARC is predominantly influenced by the properties of the working pairs [3]. Commonly used working pairs in an ARC include H_2O/LiBr and NH_3/H_2O. However, the drawbacks of pairs are obvious, such as corrosion, crystallization, high operating pressures, and toxicity [4]. Consequently, the exploration of novel working pairs capable of addressing these limitations has attracted more and more attention in recent years.

Ionic liquids (ILs), also known as room-temperature molten salts, are novel compounds composed of organic cations and inorganic or organic anions that remain in a liquid state at ambient temperatures. ILs exhibit excellent thermal stability, low flammability, and extremely low vapor pressure [5,6]. These properties make it a promising potential absorbent for the ARC. Wu et al. compared the performance of ARCs using different

ILs as absorbents, including [emim][BF_4], [hmim][BF_4], [omim][BF_4], and [hmim][Tf_2N], and found that the HFO-1234ze(E)/[hmim][Tf_2N] pair has the highest performance (COP = 0.606) [7]. In addition, Park et al. analyzed the performance of a simultaneous cooling and heating adsorption system [8], using four ILs ([dmim][DMP], [emim][DMP], [em im][BF_4], and [hmim][Tf_2N]) as absorbents and H_2O and HFC-32 as refrigerants. The results show that the HFC-32/[hmim][Tf_2N] pair has an advantage in subzero cooling temperatures, and the system size is more compact. Hence, [hmim][Tf_2N] can be considered as a good absorbent for use in the ARC.

The properties of a refrigerant/[hmim][Tf_2N] system are of importance for its application. Many researchers have studied the phase behavior of various refrigerants in [hmim][Tf_2N], as indicated in Table 1. With respect to hydrofluorocarbon (HFC) refrigerants, Ren and Scurto [9] measured the vapor–liquid equilibrium (VLE) of HFC-134a with [hmim][Tf_2N] at temperatures of 298.15 K~348.15 K and pressures up to 1.8 MPa. The results reveal that the anion has a greater influence on solubility than the cation. Liu et al. [10] systematically investigated the solubility of HFC refrigerants (HFC-32, HFC-152a, HFC-125, HFC-161, HFC-143a, HFC-245fa, HFC-236fa, and HFC-227ea) in [hmim][Tf_2N] in the temperature range of 302 K to 344 K. In addition, Liu et al. [11,12] also reported the solubility of hydrofluoroolefin (HFO) refrigerants such as HFO-1234ze(E), HFO-1234yf, and HFO-1233zd(E) in [hmim][Tf_2N] over a temperature range of 293 K to 353 K and pressures up to 0.93 MPa. The results show that HFO-1234ze(E) exhibits higher solubility than HFO-1234yf, and the two refrigerants show greater solubility in [hmim][Tf_2N] than HFC refrigerants.

Table 1. Summary of the solubility of refrigerants in [hmim][Tf_2N].

Refrigerants	Authors	Years	*T*/K	*p*/MPa	Mole Fraction x_1
HFC-134a	Ren and Scurto [9]	2009	298.15–343.15	0.042–1.878	0.0247–0.7642
HFC-227ea	Liu et al. [13]	2018	303.15–343.15	0.058–0.485	0.042–0.284
HFC-236fa	Liu et al. [13]	2018	303.15–343.15	0.030–0.315	0.046–0.279
HFC-245fa	Liu et al. [13]	2018	303.15–343.15	0.016–0.144	0.049–0.196
HFC-143a	Liu et al. [14]	2015	302.7–343.0	0.130–1.545	0.0434–0.3561
HFC-125	Liu et al. [10]	2015	302.6–332.8	0.1091–0.9172	0.0576–0.3282
HFC-152a	Liu et al. [10]	2015	302.3–343.4	0.0376–0.3074	0.0573–0.2528
HFC-161	Liu et al. [14]	2015	302.2–344.3	0.030–0.673	0.0305–0.3878
HFC-32	Liu et al. [10]	2015	302.5–344.1	0.1144–1.2208	0.0923–0.4972
HFO-1233zd(E)	He et al. [12]	2018	303.12–343.17	0.009–0.130	0.010–0.113
HFO-1234ze(E)	Liu et al. [11]	2016	292.98–353.23	0.0497–0.6937	0.0228–0.3312
HFO-1234yf	Liu et al. [11]	2016	292.29–353.21	0.0993–0.9251	0.0376–0.3536
HC-600a	Liu et al. [15]	2015	303.2–343.5	0.0482–0.4524	0.014–0.103
HC-50	Kumelan et al. [16]	2007	293.3–413.25	0.886–9.300	0.0632–0.5106 *
HC-170	Henni et al. [17]	2024	303.15–343.15	0.0199–1.3009	0.003–0.139
HC-50	Anderson et al. [18]	2007	298.15–333.15	0.0202–0.988	0.00116–0.0246
HC-170	Florusse et al. [19]	2008	293.19–368.40	0.388–13.070	0.0995–0.4016
RC-270	Liu et al. [15]	2015	303.5–343.3	0.1473–1.1578	0.028–0.206
CO_2	Henni et al. [20]	2022	303.15–343.15	0.0195–1.4009	0.005–0.311
CO_2	Shokouhi et al. [21]	2023	313.15–353.15	0.265–0.843	0.053–0.155
CO_2	Yim et al. [22]	2013	303.15–373.15	0.42–45.28	0.165–0.824
CO_2	Kumelan et al. [23]	2006	293.15–413.2	0.601–9.911	0.2459–4.6574 *
CO_2	Aki et al. [24]	2004	298.1–333.3	1.315–11.558	0.1993–0.7586
CO_2	Shiflett et al. [25]	2007	281.9–348.6	0.0089–1.9764	0.001–0.539

* indicates that the unit is mol/kg.

Considering the environmental issues they pose, HFC refrigerants with high global warming potential (GWP) will be phased out, as required by the Kigali Amendment to

the Montreal Protocol. Among the potential alternatives, hydrocarbon (HC) refrigerants have emerged as highly promising, owing to their zero ozone depletion potential (ODP), low GWP, high latent heat of evaporation, and superior cooling capacity [26]. For example, HC-290 has been considered as a good alternative refrigerant for use in household air conditioners due to its good thermophysical properties [27]. In order to explore the possibility of using HC-290 in the ARC, Al-Dadah et al. [28] studied the performance of a solar-assisted vapor absorption system using HC-290 as a refrigerant and AB300 lubricant as an absorbent. In addition, Liu et al. [29] and Sun et al. [30] investigated the phase equilibria of HC-290 with [hmim][FEP] and [P_{66614}] Cl ILs to provide the essential data for the performance analysis of the ARC. However, to this author's knowledge, there are no reports on the properties of an HC-290/[hmim][Tf_2N] mixture. To address this research gap, this study investigates the solubility of HC-290 in [hmim][Tf_2N] over a temperature range of 283.15 K to 343.15 K utilizing the isochoric saturation method. Furthermore, a comparative analysis is conducted to evaluate the solubility and absorption performance of [hmim][Tf_2N] with various refrigerants.

2. Experimental Method

2.1. Experimental Samples

The HC-290 (CAS No.: 74-98-6) used in this work was provided by Yonghe Refrigerant Co., Ltd. (Zhejiang, China), with a mass purity higher than 99.95%. [hmim][Tf_2N] (CAS No.: 382150-50-7) was supplied by Chengjie Chemical Co., Ltd. (Shanghai, China) with a claimed mass purity of 98%. Before use, it was dried under vacuum at 348.15 K for 72 h to remove trace water impurities. The final water content was measured using an MKC-710B Karl Fischer titrator (Kyoto, Japan) and lower than 100 ppm. The chemical structures of HC-290 and [hmim][Tf_2N] are shown in Figure 1.

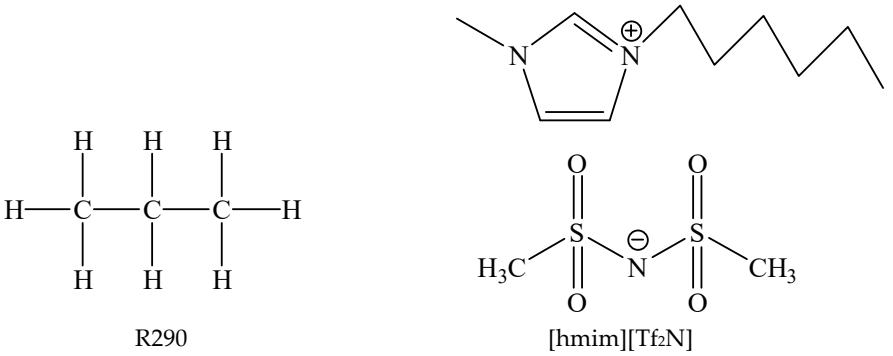


Figure 1. Chemical structures of HC-290 and [hmim][Tf_2N].

2.2. Experimental Setup

Due to the extremely low vapor pressure of [hmim][Tf_2N], as indicated by Sarafov et al. [31], the isochoric saturation method is suitable for measuring the solubility of HC-290 in [hmim][Tf_2N]. A schematic diagram of the experimental system established based on the isochoric saturation method is shown in Figure 2. Detailed information about the experimental system is given in our previous work [32,33]. Here, a brief introduction is given. The core part of the experimental system is the gas chamber and the equilibrium cell, as shown in Figure 2. The volume of the gas chamber and the equilibrium cell was calibrated using carbon dioxide, and the values were 103.61 cm^3 and 33.37 cm^3 [34], respectively. The gas chamber and equilibrium cell are located in the thermostat bath, and the temperature of the bath was measured using a 100 Ω platinum resistance thermometer produced by Fluke (USA, model: Fluke 5608, accuracy: 0.01 K). In addition, the temperature of the bath was

maintained constant through a Lauda ECO temperature controller, and the refrigeration system cooled the bath through the heat exchanger.

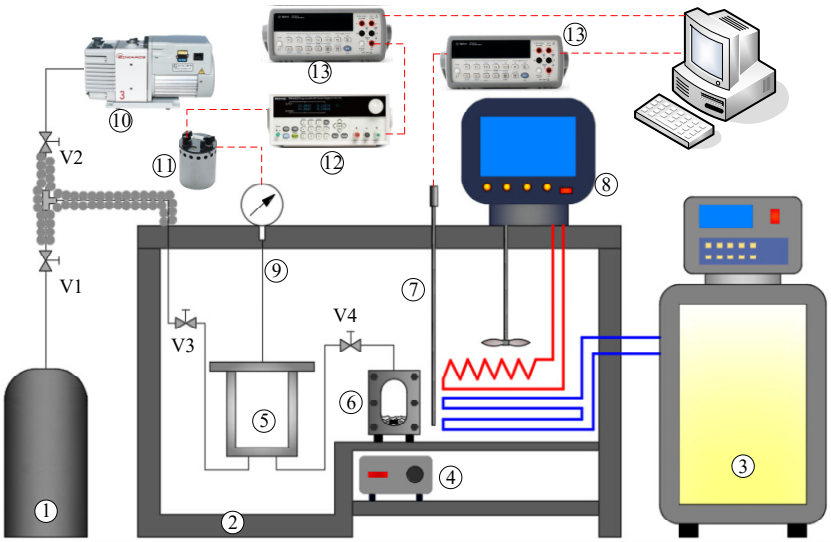


Figure 2. Schematic diagram of the experimental solubility system. 1: gas cylinder; 2: water thermostat bath; 3: refrigeration system; 4: magnetic stirrer; 5: gas chamber; 6: equilibrium cell; 7: thermometer; 8: temperature controller; 9: pressure sensor; 10: vacuum pump; 11: resistance; 12: DC power supply; 13: multimeter.

According to the principle of the isochoric saturation method, the pressure change in the gas chamber should be measured. Therefore, the pressure was measured using a Keller pressure sensor (Switzerland) with a maximum range of 3 MPa (model: Keller 33X, accuracy: 0.03% FS). The expanded uncertainties of the temperature and pressure measurement were estimated, and the values were less than 0.03 K and 2.0 kPa (k = 2), respectively.

Before the measurement, a specific amount of [hmim][Tf_2N] was injected into the equilibrium cell, and the injected weight was determined using an analytical balance (Mettler Toledo, Switzerland, model: ME204, accuracy: ±0.0002 g). Once the vacuum treatment of the system was completed and the temperature of the thermostat bath was stabilized, HC-290 was released into the gas chamber. The initial pressure was recorded when the pressure stabilized. Subsequently, valve V4 (as shown in Figure 2) was opened to allow the HC-290 in the gas chamber to enter into the equilibrium cell. When the pressure stabilized, the value was recorded again. The mole fraction of HC-290 dissolved in [hmim][Tf_2N] could be calculated based on the pressure change and temperature.

The mole fraction (x_1) of HC-290 in [hmim][Tf_2N] is calculated as:

$$x_1 = \frac{n_1}{n_1 + n_2} \tag{1}$$

$$n_2 = \frac{m_2}{M_2} \tag{2}$$

where n_2 represents the mole number of [hmim][Tf_2N], which can be obtained from its mass, m_2 (4.1306 g), in the equilibrium cell and molar mass, M_2 (447.41 g/mol). n_1 represents the mole number of HC-290 dissolved in [hmim][Tf_2N]. Based on the mass conservation of HC-290 in the system, n_1 can be obtained using the following equation [34]:

$$n_1 = n_1^0 - n_1^1 = \rho_1^0 V_{gc} - \rho_1^1 \left(V_{gc} + V_{ec} - V_{1,liquid} - V_{IL} \right) \tag{3}$$

where n_1^0 and n_1^1 are the mole number of vapor HC-290 in the initial condition and the equilibrium condition, respectively. ρ_1^0 and ρ_1^1 are the molar density of vapor HC-290 in the initial condition and the equilibrium condition. The values were obtained from Refprop 10.0 [35]. V_{gc} and V_{ec} represent the volumes of the gas chamber and the equilibrium cell, respectively. V_{IL} is the volume of [hmim][Tf_2N] in the equilibrium cell, which was obtained from the injected mass and liquid density [29]. $V_{1,liquid}$ is the liquid volume of HC-290 dissolved in [hmim][Tf_2N] and can be calculated by:

$$V_{1,liquid} = n_1 / \rho_{1,liquid}^1 \tag{4}$$

where $\rho_{1,liquid}^1$ is the liquid density of HC-290. Combined with Equations (3) and (4), the mole number of HC-290 dissolved in [hmim][Tf_2N] can be calculated via:

$$n_1 = \left[\rho_1^0 V_{gc} - \rho_1^1 (V_{gc} + V_{ec} - V_{IL})\right] / \left(1 - \rho_1^1 / \rho_{1,liquid}^1\right) \tag{5}$$

According to the uncertainty propagation [36], the combined expanded uncertainty of the mole fraction can be calculated by:

$$U(x_1) = k \cdot \sqrt{\left(\frac{\partial x_1}{\partial n_1}\right)^2 \cdot u^2(n_1) + \left(\frac{\partial x_1}{\partial n_2}\right)^2 \cdot u^2(n_2)} \tag{6}$$

where k is the coverage factor (k = 2 in this work). $u(n_1)$ and $u(n_2)$ are the uncertainties of the mole number of HC-290 and [hmim][Tf_2N]:

$$u(n_1) = \sqrt{\begin{array}{l}\left(\frac{\partial n_1}{\partial \rho_1^0}\right)^2 \cdot u^2(\rho_1^0) + \left(\frac{\partial n_1}{\partial \rho_1^1}\right)^2 \cdot u^2(\rho_1^1) + \left(\frac{\partial n_1}{\partial \rho_{1,liquid}^1}\right)^2 \cdot u^2\left(\rho_{1,liquid}^1\right) \\ + \left(\frac{\partial n_1}{\partial V_{gc}}\right)^2 \cdot u^2(V_{gc}) + \left(\frac{\partial n_1}{\partial V_{ec}}\right)^2 \cdot u^2(V_{ec}) + \left(\frac{\partial n_1}{\partial V_{IL}}\right)^2 \cdot u^2(V_{IL})\end{array}} \tag{7}$$

$$u(n_2) = \sqrt{\left(\frac{\partial n_2}{\partial m_2}\right)^2 \cdot u^2(m_2)} \tag{8}$$

The uncertainty for each parameter is given in Table 2. The calculated results show that the combined relative expanded uncertainty of the mole fraction $U_r(x_1)$ was less than 2.78% (k = 2).

Table 2. Sources of uncertainty for each parameter.

Source of Uncertainty	Relative Value	Source of Uncertainty	Relative Value
$u(\rho_1)$	0.03%	$u(m_2)$	0.001%
$u(\rho_{1,liquid}^1)$	0.01%	$u(V_{gc})$	0.1%
$u(V_{IL})$	0.05%	$u(V_{ec})$	0.1%

3. Experimental Results and Discussion

In order to validate the reliability of the experimental system, the solubility of carbon dioxide in pentaerythritol tetraoctanoate (Abbreviate as PEC8, CAS:3008-50-2) and HFO-1234yf in [hmim][TfO] (CAS:460345-16-8) was measured at 303.15 K, and the results were compared with those from the literature [37,38]. The maximum deviation between this work and literature was 2.50%, indicating that the experimental system has good reliability, as indicated in Figure 3.

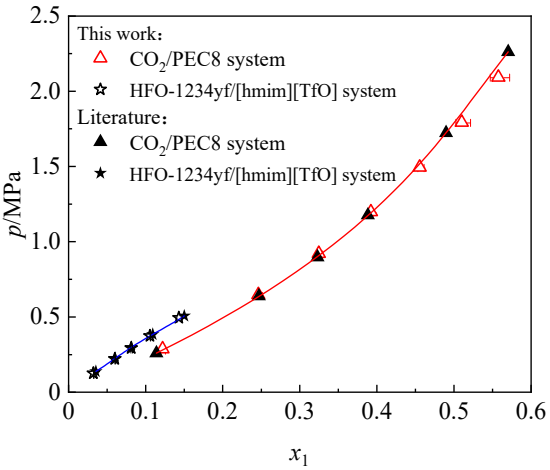


Figure 3. Solubility comparison between this work and the literature at 303.15 K for CO_2/PEC8 and HFO-1234yf/[hmim][TfO] system.

3.1. Experimental Data and Correlation

In this work, the solubility of HC-290 in [hmim][Tf_2N] was measured in the temperature range of 283.15 K to 343.15 K, which corresponds to the typical temperature range of an ARC. It should be noted that the maximum pressure here was 0.428 MPa; this is because the equilibrium cell was designed with a glass observation window, and the pressure resistance of the cell was limited to within 0.6 MPa. The experimental data are listed in Table 3, and the trends of the mole fraction of HC-290 at different temperatures and pressures are given in Figure 4. As expected, the absorption capacity of [HMIM][Tf_2N] for HC-290 increased with decreasing temperature and increasing pressure. Moreover, HC-290 and [HMIM][Tf_2N] were completely miscible within the experimental temperature and pressure ranges.

Table 3. Experimental data on the solubility of HC-290 in [HMIM][Tf_2N].

***p*/MPa**	**x_1**	***p*/MPa**	**x_1**	***p*/MPa**	**x_1**	***p*/MPa**	**x_1**
283.15 K		293.15 K		303.15 K		313.15 K	
0.121	0.068	0.129	0.058	0.135	0.050	0.142	0.044
0.160	0.088	0.170	0.074	0.179	0.064	0.188	0.05
0.198	0.106	0.211	0.091	0.222	0.077	0.233	0.067
0.236	0.125	0.251	0.106	0.265	0.091	0.278	0.079
0.280	0.148	0.298	0.125	0.314	0.106	0.330	0.092
0.319	0.166	0.340	0.141	0.359	0.120	0.378	0.103
323.15 K		333.15 K		343.15 K			
0.148	0.038	0.155	0.033	0.161	0.029		
0.197	0.048	0.205	0.042	0.213	0.037		
0.244	0.058	0.254	0.051	0.264	0.045		
0.290	0.069	0.303	0.061	0.315	0.053		
0.346	0.080	0.360	0.071	0.375	0.062		
0.395	0.091	0.412	0.081	0.428	0.072		

The non-random two-liquid (NRTL) model and Krichevsky–Kasarnovsky (K-K) model were used to correlate the obtained solubility data in this work. The expression of the NRTL model is [39]:

$$\ln \gamma_1 = x_2^2 \left[\tau_{21} \left(\frac{\exp(-\alpha\tau_{21})}{x_1 + x_2 \exp(-\alpha\tau_{21})} \right)^2 + \frac{\tau_{12} \exp(-\alpha\tau_{12})}{[x_2 + x_1 \exp(-\alpha\tau_{12})]^2} \right] \quad (9)$$

$$\ln \gamma_2 = x_1^2 \left[\tau_{12} \left(\frac{\exp(-\alpha\tau_{12})}{x_2 + x_1 \exp(-\alpha\tau_{12})} \right)^2 + \frac{\tau_{21} \exp(-\alpha\tau_{21})}{[x_1 + x_2 \exp(-\alpha\tau_{21})]^2} \right] \quad (10)$$

where x_1 and x_2 are the mole fraction of HC-290 and [hmim][Tf_2N] in the liquid mixture in the equilibrium condition. γ_1 is the activity coefficient of HC-290 in the liquid phase. γ_2 is the activity coefficient of [hmim][Tf_2N]. τ_{12} and τ_{21} are the binary interaction parameters, which were calculated using the following expression:

$$\tau_{12} = \tau_{12,0} + \tau_{12,1}(T - 273.15) + \tau_{12,2}(T - 273.15)^2 \quad (11)$$

$$\tau_{21} = \tau_{21,0} + \tau_{21,1}(T - 273.15) + \tau_{21,2}(T - 273.15)^2 \quad (12)$$

Here, α, $\tau_{21,0}$, $\tau_{21,1}$, $\tau_{21,2}$, $\tau_{12,0}$, $\tau_{12,1}$, and $\tau_{12,2}$ are coefficients obtained through experimental data.

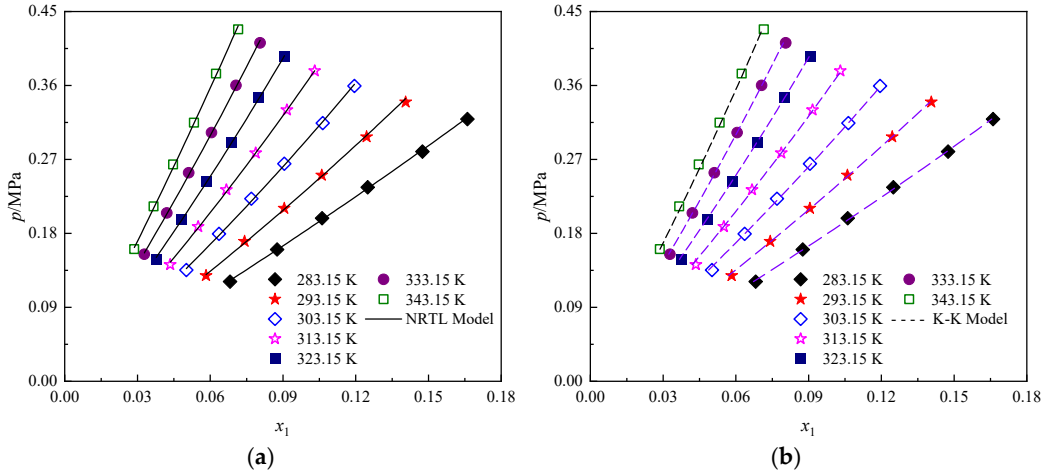


Figure 4. Mole fraction of HC-290 in [hmim][Tf_2N] at different temperatures and pressures. (**a**) NRTL model. (**b**) K-K model.

With respect to the activity coefficient of HC-290 in the liquid phase, γ_1, it can be calculated from the vapor–liquid equilibrium (VLE) relationship [40]:

$$\gamma_1 x_1 p_1^s = \zeta_1 y_1 p \quad (13)$$

where $p_1{}^s$ is the saturation vapor pressure of HC-290, and p is the pressure of the HC-290/[hmim][Tf_2N] mixture in the equilibrium condition. y_1 represents the mole fraction of HC-290 in the vapor phase. Due to the extremely low vapor pressure of [hmim][Tf_2N] [31], y_1 is assumed to be 1 here. ζ_1 is the correction factor:

$$\zeta_1 = \exp\left[\frac{(B_1 - v_1)(p - p_1^s)}{RT} \right] \quad (14)$$

where B_1 is the second virial coefficient, v_1 is the molar volume of HC-290 in the liquid phase, and R is the universal gas constant. B_1, $p_1{}^s$, and v_1 are obtained from Refprop 10.0 [35].

In the K-K model, the expression for the liquid-phase mole fraction (x_1) of HC-290 is given as follows [41]:

$$\ln\left(\frac{f_1}{x_1}\right) = \ln He + \frac{v_1^\infty p}{RT} \quad (15)$$

where f_1 represents the fugacity of HC-290 at a given temperature and pressure. ${v_1}^{\infty}$ denotes the infinite dilution molar volume of HC-290, and *He* represents the Henry's law constant. *He* and ${v_1}^{\infty}$ can be determined using the following equations:

$$\ln He = A_0 + \frac{A_1}{T} \tag{16}$$

$$v_1^{\infty} = B_0 + B_1 T + B_2 T^2 \tag{17}$$

The coefficients A_0, A_1, B_0, B_1, and B_2 are regressed from the experimental results. The optimized coefficients in the NRTL model and K-K model are listed in Table 4.

Table 4. Optimized coefficients in NRTL model and K-K model.

Parameters	Values	Parameters	Values
α	−0.0172	A_0	7.001
$\tau_{12,0}$	17.726	A_1	−1827
$\tau_{12,1}$	−0.0132	B_0	−11,044
$\tau_{12,2}$	1.0963	B_1	70.97
$\tau_{21,0}$	−23.0298	B_2	−0.1087
$\tau_{21,1}$	0.02296		
$\tau_{21,2}$	−0.00000423		

The deviation distribution between the calculated values from the model and experimental data for the liquid-phase mole fraction is presented in Figure 5. For the NRTL and K-K models, the average absolute relative deviations (AARDs) were 0.76% and 0.78%, respectively. The maximum relative deviations (MRDs) were 3.40% and 3.24%. The AARD and MRD were calculated according to the equations shown below.

$$AARD = \frac{\sum_{i}^{n} \left| (x_{\text{cal}} - x_{\text{exp}}) / x_{\text{exp}} \right|}{n} \times 100\% \tag{18}$$

$$MRD = \max\left(\left| \frac{(x_{\text{cal},i} - x_{\text{exp},i})}{x_{\text{exp},i}} \right| \right) \times 100\% \tag{19}$$

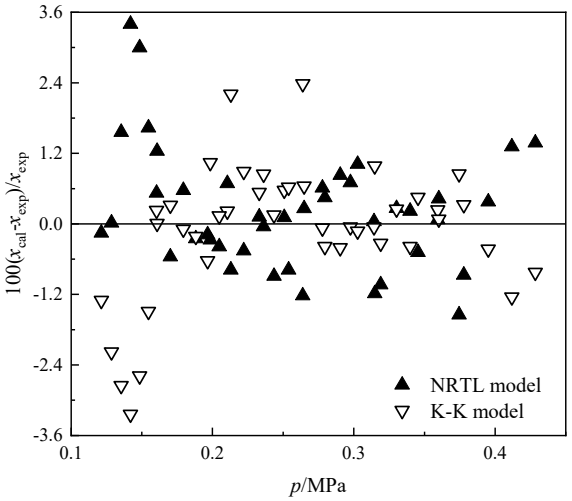


Figure 5. Deviations between experimental data and calculated results from NRTL model and K-K model.

3.2. Derived Thermodynamic Properties of HC-290/[hmim][Tf_2N]

To better understand the dissolution process of HC-290 in [hmim][Tf_2N], it was necessary to analyze the derived thermodynamic properties, such as enthalpy change (Δh_{total}) and entropy change (Δs_{total}). Typically, the dissolution of a gaseous solute in a liquid solvent at a given temperature occurs in two steps. In the first step, HC-290 condenses from the gas phase to a saturated liquid phase. The change in enthalpy (Δh_{con}) and entropy (Δs_{con}) in the condensation process can be obtained from REFPROP 10.0 [35]. In the second step, the saturated liquid HC-290 mixes with [hmim][Tf_2N], resulting in mixing enthalpy (Δh_{mixing}), mixing Gibbs free energy (Δg_{mixing}), and mixing entropy (Δs_{mixing}). The total enthalpy (Δh_{total}) and total entropy (Δs_{total}) for the entire dissolution process can be calculated using the following equations:

$$\Delta h_{total} = \Delta h_{con} + \Delta h_{mixing} \quad (20)$$

$$\Delta s_{total} = \Delta s_{con} + \Delta s_{mixing} \quad (21)$$

For an ideal solution, the expressions for the properties (Δh^{ideal}, Δg^{ideal}, and Δs^{ideal}) are:

$$\Delta h^{ideal} = 0 \quad (22)$$

$$\Delta g^{ideal} = RT(x_1 \ln x_1 + x_2 \ln x_2) \quad (23)$$

$$\Delta s^{ideal} = -R(x_1 \ln x_1 + x_2 \ln x_2) \quad (24)$$

For a real solution, the values of the derived thermodynamic properties are the sum of the ideal properties and the excess properties:

$$\Delta h_{mixing} = \Delta h^{ideal} + \Delta h^{excess} \quad (25)$$

$$\Delta g_{mixing} = \Delta g^{ideal} + \Delta g^{excess} \quad (26)$$

$$\Delta s_{mixing} = \Delta s^{ideal} + \Delta s^{excess} \quad (27)$$

The expressions for the excess thermodynamic properties (Δh^{excess}, Δg^{excess}, and Δs^{excess}) can be calculated based on the NRTL model:

$$\Delta h^{excess} = -RT^2\left[\frac{\partial(\Delta g^{excess}/RT)}{\partial T}\right] = -RT^2\left[x_1\frac{\partial(\ln\gamma_1)}{\partial T} + x_2\frac{\partial(\ln\gamma_2)}{\partial T}\right] \quad (28)$$

$$\Delta g^{excess} = RT\sum x_i \ln\gamma_i = RT(x_1 \ln\gamma_1 + x_2 \ln\gamma_2) \quad (29)$$

$$\Delta s^{excess} = \frac{\Delta h^{excess} - \Delta g^{excess}}{T} \quad (30)$$

where γ_1 is the activity coefficient of HC-290 in the liquid phase and γ_2 is the activity coefficient of [hmim][Tf_2N].

Based on experimental solubility data and the NRTL model, the values of Δh_{con}, Δs_{con}, Δh_{mixing}, Δg_{mixing}, Δs_{mixing}, Δh_{total}, and Δs_{total} were calculated, and the results are listed in Table 5. The variations in mixing Gibbs free energy, total entropy change, and total enthalpy changed with respect to the mole fraction, and are shown in Figure 6.

Table 5. The calculated results of Δh_{con}, Δs_{con}, Δh_{mixing}, Δg_{mixing}, Δs_{mixing}, Δh_{total}, and Δs_{total} for HC-290/[hmim][Tf_2N] system.

T/K	x_1	Δh_{con}	Δs_{con}	Δh_{mixing}	Δg_{mixing}	Δs_{mixing}	Δh_{total}	Δs_{total}
		/J·mol^{-1}	/J·mol^{-1}·K^{-1}	/J·mol^{-1}	/J·mol^{-1}	/J·mol^{-1}·K^{-1}	/J·mol^{-1}	/J·mol^{-1}·K^{-1}
283.15	0.068	−15,887.91	−56.11	21.37	−411.64	1.53	−15,866.54	−54.58
283.15	0.088	−15,887.91	−56.11	35.15	−473.60	1.80	−15,852.75	−54.32
283.15	0.106	−15,887.91	−56.11	49.75	−518.50	2.01	−15,838.15	−54.11
283.15	0.125	−15,887.91	−56.11	67.07	−556.78	2.20	−15,820.84	−53.91
283.15	0.148	−15,887.91	−56.11	90.17	−592.70	2.41	−15,797.73	−53.70
283.15	0.166	−15,887.91	−56.11	109.56	−614.12	2.56	−15,778.35	−53.56
293.15	0.058	−15,184.07	−51.80	1.62	−388.41	1.33	−15,182.45	−50.46
293.15	0.074	−15,184.07	−51.80	8.16	−447.58	1.55	−15,175.91	−50.24
293.15	0.091	−15,184.07	−51.80	17.43	−499.74	1.76	−15,166.64	−50.03
293.15	0.106	−15,184.07	−51.80	27.38	−538.19	1.93	−15,156.69	−49.87
293.15	0.125	−15,184.07	−51.80	42.05	−578.38	2.12	−15,142.02	−49.68
293.15	0.141	−15,184.07	−51.80	55.95	−605.91	2.26	−15,128.12	−49.54
303.15	0.05	−14,407.91	−47.52	−14.70	−366.20	1.16	−14,422.61	−46.36
303.15	0.064	−14,407.91	−47.52	−13.39	−425.78	1.36	−14,421.31	−46.16
303.15	0.077	−14,407.91	−47.52	−10.38	−473.13	1.53	−14,418.29	−46.00
303.15	0.091	−14,407.91	−47.52	−5.37	−517.00	1.69	−14,413.28	−45.83
303.15	0.106	−14,407.91	−47.52	1.84	−557.06	1.84	−14,406.07	−45.68
303.15	0.12	−14,407.91	−47.52	10.12	−588.88	1.98	−14,397.79	−45.55
313.15	0.044	−13,541.35	−43.24	−28.54	−347.83	1.02	−13,569.89	−42.22
313.15	0.05	−13,541.35	−43.24	−30.32	−377.55	1.11	−13,571.66	−42.13
313.15	0.067	−13,541.35	−43.24	−32.93	−451.02	1.34	−13,574.27	−41.90
313.15	0.079	−13,541.35	−43.24	−32.76	−494.96	1.48	−13,574.11	−41.76
313.15	0.092	−13,541.35	−43.24	−30.87	−536.45	1.61	−13,572.22	−41.63
313.15	0.103	−13,541.35	−43.24	−27.98	−567.26	1.72	−13,569.33	−41.52
323.15	0.038	−12,562.33	−38.87	−39.87	−324.78	0.88	−12,602.20	−37.99
323.15	0.048	−12,562.33	−38.87	−46.53	−378.42	1.03	−12,608.86	−37.85
323.15	0.058	−12,562.33	−38.87	−51.76	−425.83	1.16	−12,614.09	−37.72
323.15	0.069	−12,562.33	−38.87	−55.94	−471.99	1.29	−12,618.27	−37.59
323.15	0.08	−12,562.33	−38.87	−58.59	−512.83	1.41	−12,620.91	−37.47
323.15	0.091	−12,562.33	−38.87	−59.79	−549.06	1.51	−12,622.12	−37.36
333.15	0.033	−11,431.60	−34.31	−49.13	−302.99	0.76	−11,480.74	−33.55
333.15	0.042	−11,431.60	−34.31	−59.12	−356.24	0.89	−11,490.73	−33.42
333.15	0.051	−11,431.60	−34.31	−67.78	−403.63	1.01	−11,499.38	−33.31
333.15	0.061	−11,431.60	−34.31	−75.90	−450.60	1.12	−11,507.50	−33.19
333.15	0.071	−11,431.60	−34.31	−82.52	−492.50	1.23	−11,514.13	−33.08
333.15	0.081	−11,431.60	−34.31	−87.74	−530.03	1.33	−11,519.34	−32.99
343.15	0.029	−10,082.14	−29.38	−57.03	−310.39	0.66	−10,139.17	−28.72
343.15	0.037	−10,082.14	−29.38	−69.77	−364.90	0.77	−10,151.91	−28.61
343.15	0.045	−10,082.14	−29.38	−81.31	−413.40	0.88	−10,163.46	−28.51
343.15	0.053	−10,082.14	−29.38	−91.70	−461.48	0.97	−10,173.85	−28.42
343.15	0.062	−10,082.14	−29.38	−102.07	−504.39	1.06	−10,184.21	−28.32
343.15	0.072	−10,082.14	−29.38	−112.02	−542.84	1.16	−10,194.16	−28.23

Both Δh_{total} and Δs_{total} exhibited negative values, indicating that the dissolution process of HC-290 in [hmim][Tf_2N] is an exothermic process. Furthermore, the positive value of Δs_{mixing} suggests that the mixing process of HC-290 with [hmim][Tf_2N] is thermodynamically irreversible. However, Δh_{mixing} did not follow a strictly positive or negative trend. This phenomenon can be primarily attributed to two competing effects. On one hand, the dissolution of HC-290 in [hmim][Tf_2N] disrupts the hydrogen bonding network and ionic interactions within the ionic liquid, necessitating energy absorption and resulting in an endothermic contribution. On the other hand, according to van der Waals interactions and Lewis acid−base theory [42], the intermolecular interactions between the refrigerant and the ionic liquid introduce an exothermic effect. The balance between these opposing thermodynamic effects determines the overall sign of Δh_{mixing}. As illustrated in

Figure 6, the Gibbs free energy of mixing ΔG_{mixing} for HC-290 in [hmim][Tf_2N] remains negative and decreases with increasing temperature, indicating that the dissolution process is thermodynamically spontaneous and becomes more favorable as temperature rises.

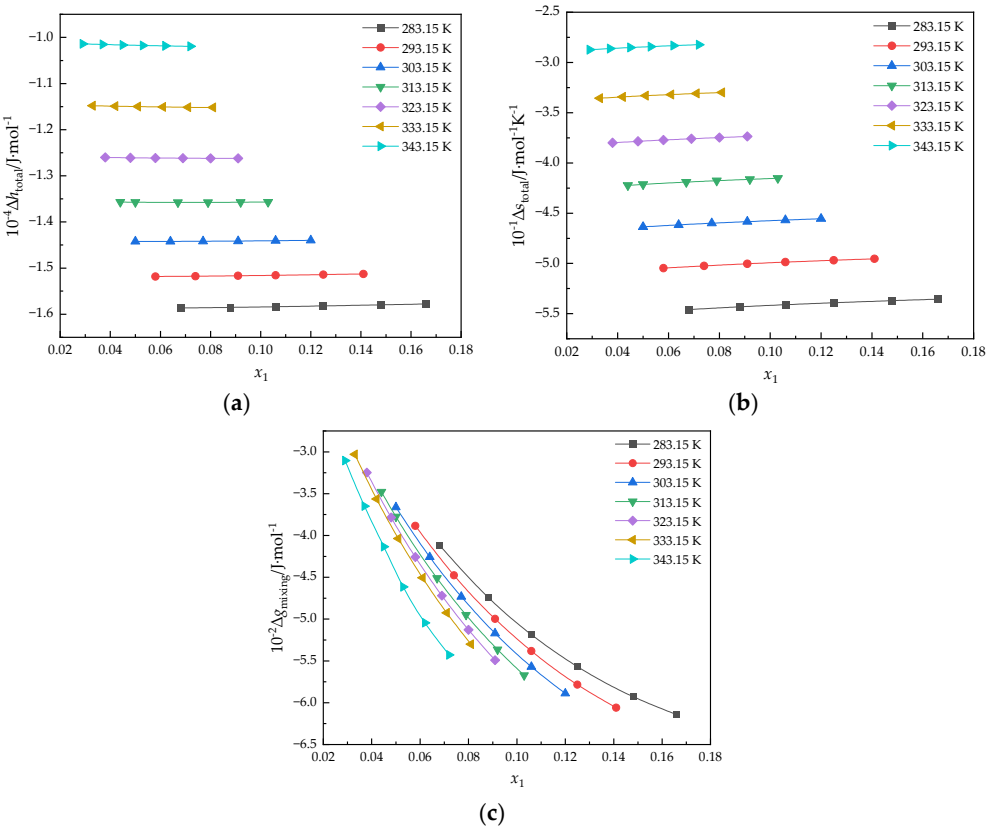


Figure 6. Variations in enthalpy change, entropy change, and mixing Gibbs free energy with liquid−phase mole fraction of HC-290 in [hmim][Tf_2N]. (**a**) Enthalpy change. (**b**) Entropy change. (**c**) Mixing Gibbs free energy.

3.3. Comparison of the Solubility of Different Refrigerants in [hmim][Tf_2N]

To systematically evaluate the absorption performance of [hmim][Tf_2N] with various refrigerants, the experimental data on the solubility of 16 refrigerants, including HFCs [10,12,13], HFOs [11,14], HCs [15,17,19], and CO_2 [21], in [hmim][Tf_2N] reported in the literature were summarized in this work. The Henry's constants of these refrigerants at 313.15 K and 333.15 K were calculated and compared, as indicated in Figure 7.

With respect to HC refrigerants, it can be observed that at 313.15 K, the Henry's constant followed the order: HC-170 > HC-290 > RC-270 > HC-600a. However, at 333.15 K, the values followed the order: HC-170 > RC-270> HC-290 > HC-600a. This indicates that the solubility of RC-270 in [hmim][Tf_2N] exhibits greater temperature sensitivity. In addition, in comparing the *He* values of HC-170, HC-290, and HC-600a in [hmim][Tf_2N], it can be concluded that the Henry's constant increases as the carbon number decreases. Additionally, it was observed that most HFO and HFC refrigerants exhibited lower *He* values compared to the HC refrigerants, meaning that [hmim][Tf_2N] has a higher absorption capacity for HFOs and HFCs than HCs.

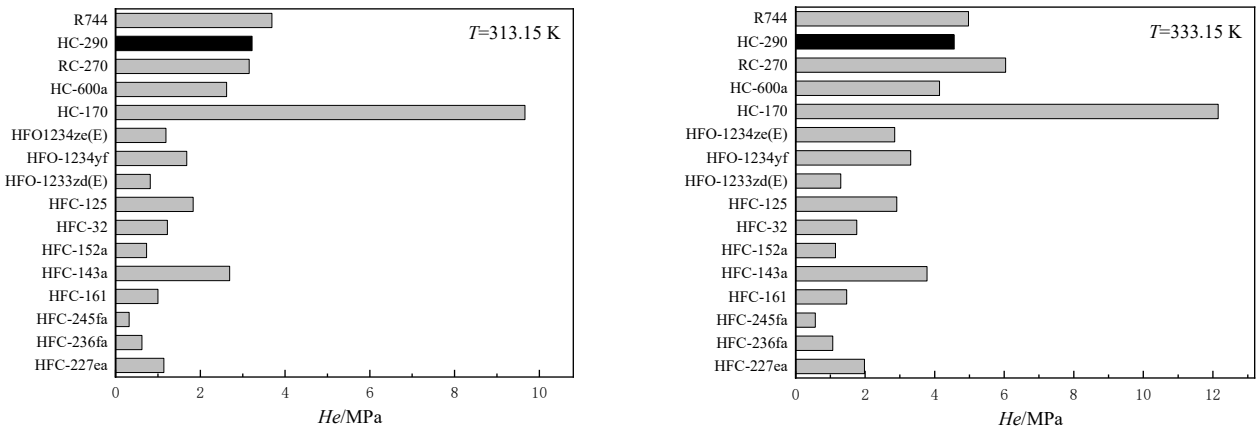


Figure 7. Henry's constants of different refrigerants in [hmim][Tf_2N] at different temperatures. (**a**) 313.15 K. (**b**) 333.15 K.

4. Conclusions

In this work, the solubility of HC-290 in [hmim][Tf_2N] was reported over a temperature range of 283.15 K to 343.15 K and pressures up to 0.428 MPa. The experimental data were correlated using the NRTL model and the K-K model. Both the NRTL and K-K models provided excellent correlative results with absolute average relative deviations of 0.76% and 0.78%, respectively. The Gibbs free energy, enthalpy change, and entropy change during the dissolution process of HC-290 in [hmim][Tf_2N] were calculated based on the NRTL model. The results confirm that the dissolution process is spontaneous, exothermic, and not entropy-driven. The Henry's constants of 16 refrigerants (including HCs, HFCs, HFOs, CO_2) in [hmim][Tf_2N] at 313.15 K and 333.15 K were calculated and compared. The results show that HFOs and HFCs exhibited lower *He* values compared to HCs.

This work provides valuable solubility data for HC-290 in [hmim][Tf_2N] for the first time, filling this gap and offering essential insights into the behavior of this refrigerant in ionic liquids. Ionic liquids, as promising green solvents, are considered key materials for low-emission, sustainable refrigeration technologies. The findings contribute to a better understanding of HC-290′s potential in enhancing the performance and environmental sustainability of refrigeration systems.

Author Contributions: Conceptualization, W.S. and X.W.; methodology, W.S.; formal analysis, W.S.; investigation, W.S. and J.S.; data curation, J.S.; writing—original draft preparation, W.S.; writing—review and editing, X.W.; visualization, W.S. and J.S.; supervision, X.W. All authors have read and agreed to the published version of the manuscript.

Funding: This research was funded by National Natural Science Foundation of China (grant number 52276165).

Data Availability Statement: The original contributions presented in this study are included in the article. Further inquiries can be directed to the corresponding author(s).

Conflicts of Interest: The authors declare no conflicts of interest.

References

1. Srikhirin, P.; Aphornratana, S.; Chungpaibulpatana, S. A review of absorption refrigeration technologies. *Renew. Sustain. Energy Rev.* **2001**, *5*, 343–372.
2. Wang, R.; Oliveira, R. Adsorption refrigeration—An efficient way to make good use of waste heat and solar energy. *Prog. Energy Combust. Sci.* **2006**, *32*, 424–458.
3. Sun, J.; Fu, L.; Zhang, S. A review of working fluids of absorption cycles. *Renew. Sustain. Energy Rev.* **2012**, *16*, 1899–1906.

4. Wang, K.; Abdelaziz, O.; Kisari, P.; Vineyard, E.A. State-of-the-art review on crystallization control technologies for water/LiBr absorption heat pumps. *Int. J. Refrig.* **2011**, *34*, 1325–1337.
5. Earle, M.J.; Seddon, K.R. Ionic liquids. Green solvents for the future. *Pure Appl. Chem.* **2000**, *72*, 1391–1398.
6. MacFarlane, D.R.; Tachikawa, N.; Forsyth, M.; Pringle, J.M.; Howlett, P.C.; Elliott, G.D.; Davis, J.H.; Watanabe, M.; Simon, P.; Angell, C.A. Energy applications of ionic liquids. *Energy Env. Sci.* **2014**, *7*, 232–250.
7. Wu, W.; You, T.; Zhang, H.Y.; Li, X.T. Comparisons of different ionic liquids combined with trans-1,3,3,3-tetrafluoropropene (R1234ze(E)) as absorption working fluids. *Int. J. Refrig.* **2018**, *88*, 45–57.
8. Park, S.; Choi, H.W.; Lee, J.W.; Cho, H.U.; Lee, N.S.; Kang, Y.T. Performance analysis of ionic liquids for simultaneous cooling and heating absorption system. *Energy* **2023**, *271*, 127005.
9. Ren, W.; Scurto, A.M. Phase equilibria of imidazolium ionic liquids and the refrigerant gas, 1,1,1,2-tetrafluoroethane (R-134a). *Fluid Phase Equilib.* **2009**, *286*, 1–7.
10. Liu, X.; He, M.; Lv, N.; Qi, X.; Su, C. Vapor−Liquid Equilibrium of Three Hydrofluorocarbons with [HMIM][Tf_2N]. *J. Chem. Eng. Data* **2015**, *60*, 1354–1361.
11. Liu, X.; Bai, L.; Liu, S.; He, M. Vapor–Liquid Equilibrium of R1234yf/[HMIM][Tf_2N] and R1234ze(E)/[HMIM][Tf_2N] Working Pairs for the Absorption Refrigeration Cycle. *J. Chem. Eng. Data* **2016**, *61*, 3952–3957. [CrossRef]
12. He, M.; Pan, P.; Yang, F.; Wang, T.; Liu, X. Gaseous Absorption of trans-1-Chloro-3,3,3-trifluoropropene in Three Immidazolium-Based Ionic Liquids. *J. Chem. Eng. Data* **2018**, *63*, 1780–1788. [CrossRef]
13. Liu, X.; Pan, P.; Yang, F.; He, M. Solubilities and diffusivities of R227ea, R236fa and R245fa in 1-hexyl-3-methylimidazolium bis(trifluoromethylsulfonyl)imide. *J. Chem. Thermodyn.* **2018**, *123*, 158–164. [CrossRef]
14. Liu, X.; He, M.; Lv, N.; Qi, X.; Su, C. Solubilities of R-161 and R-143a in 1-Hexyl-3-methylimidazolium bis(trifluoromethylsulfonyl)imide. *Fluid Phase Equilib.* **2015**, *388*, 37–42. [CrossRef]
15. Liu, X.; He, M.; Lv, N.; Qi, X.; Su, C. Solubilities of isobutane and cyclopropane in ionic liquids. *J. Chem. Thermodyn.* **2015**, *88*, 30–35. [CrossRef]
16. Kumełan, J.; Pérez-Salado Kamps, Á.; Tuma, D.; Maurer, G. Solubility of the Single Gases Methane and Xenon in the Ionic Liquid [hmim][Tf_2N]. *Ind. Eng. Chem. Res.* **2007**, *46*, 8236–8240. [CrossRef]
17. Henni, N.; Henni, A.; Ibrahim, H. Selectivities of Carbon Dioxide over Ethane in Three Methylimidazolium-Based Ionic Liquids: Experimental Data and Modeling. *Molecules* **2024**, *29*, 4152. [CrossRef]
18. Anderson, J.L.; Dixon, J.K.; Brennecke, J.F. Solubility of CO_2, CH_4, C_2H_6, C_2H_4, O_2, and N_2 in 1-Hexyl-3-methylpyridinium Bis(trifluoromethylsulfonyl)imide: Comparison to Other Ionic Liquids. *Acc. Chem. Res.* **2007**, *40*, 1208–1216. [CrossRef]
19. Florusse, L.J.; Raeissi, S.; Peters, C.J. High-Pressure Phase Behavior of Ethane with 1-Hexyl-3-methylimidazolium Bis(trifluoromethylsulfonyl)imide. *J. Chem. Eng. Data* **2008**, *53*, 1283–1285. [CrossRef]
20. Henni, N.; Henni, A.; Ibrahim, H. Solubility of carbon dioxide in promising methylimidazolium-based ionic liquids. *Fluid Phase Equilib.* **2023**, *565*, 113619. [CrossRef]
21. Shokouhi, M.; Vahidi, M.; Neshati, K.; Zhalehrajabi, E. Diffusion Coefficient and Absorption of Carbonyl Sulfide in 1-Hexyl-3-methylimidazolium Bis (Trifluoromethyl) Sulfonylimide ([hmim][Tf_2N]). *J. Chem. Eng. Data* **2023**, *68*, 586–600. [CrossRef]
22. Yim, J.H.; Lim, J.S. CO_2 solubility measurement in 1-hexyl-3-methylimidazolium ([HMIM]) cation based ionic liquids. *Fluid Phase Equilib.* **2013**, *352*, 67–74. [CrossRef]
23. Kumełan, J.; Pérez-Salado Kamps, Á.; Tuma, D.; Maurer, G. Solubility of CO_2 in the ionic liquid [hmim][Tf_2N]. *J. Chem. Thermodyn.* **2006**, *38*, 1396–1401. [CrossRef]
24. Aki, S.N.V.K.; Mellein, B.R.; Saurer, E.M.; Brennecke, J.F. High-Pressure Phase Behavior of Carbon Dioxide with Imidazolium-Based Ionic Liquids. *J. Phys. Chem. B* **2004**, *108*, 20355–20365. [CrossRef]
25. Shiflett, M.B.; Yokozeki, A. Solubility of CO_2 in Room Temperature Ionic Liquid [hmim][Tf_2N]. *J. Phys. Chem. B* **2007**, *111*, 2070–2074. [CrossRef] [PubMed]
26. Kumar, A.; Agrawal, A.; Saini, V.; Praveen Kumar, S.; Velkin, V.I.; Shcheklein, S.E. A domestic refrigerator's potential of using hydrocarbon blends as refrigerants. *J. Therm. Anal. Calorim.* **2024**, *149*, 12803–12813. [CrossRef]
27. Issa, A.B.; Liang, C.K.; Groll, E.A.; Ziviani, D. Residential heat pump and air conditioning systems with propane (R290) refrigerant: Technology review and future perspective. *App. Therm. Eng.* **2025**, *266*, 125560. [CrossRef]
28. Al-Dadah, R.K.; Jackson, G.; Rezk, A. Solar powered vapor absorption system using propane and alkylated benzene AB300 oil. *App. Therm. Eng.* **2011**, *31*, 1936–1942. [CrossRef]
29. Liu, X.Y.; Lv, N.; Bai, L.H.; He, M.G. Solubilities of propane and cyclopropane in 1-hexyl-3-methylimidazolium tris(pentafluoroethyl)trifluorophosphate. *Int. J. Refrig.* **2016**, *67*, 69–76. [CrossRef]
30. Sun, Y.J.; Wang, J.; Wei, Q.M.; Wang, X.P. Solubility for propane and isobutane in [P_{66614}]Cl from 278.15 to 348.15 K. *J. Chem. Eng. Data* **2021**, *66*, 1273–1279. [CrossRef]
31. Safarov, J.; Kul, I.; Talibov, M.; Shahverdiyev, A.; Hassel, E. Vapor pressures and activity coefficients of methanol in binary mixtures with 1-hexyl-3-methylimidazolium bis(trifluoromethysulfony)imide. *J. Chem. Eng. Data* **2015**, *60*, 1648–1663.

32. Wang, X.D.; Zhang, Y.H.; Zhi, H.Q.; Wang, X.P. Absorption separation of binary refrigerant blends using 1-butyl-3-methylimidazolium thiocyanate ionic liquid. *J. Chem. Eng. Data* **2025**, *70*, 398–407.
33. Jia, X.C.; Du, Y.H.; Wang, X.P. Selective absorption of ionic liquids in separating R-1243zf or R-161 from refrigerant blends. *J. Chem. Thermodyn.* **2024**, *196*, 107307.
34. Wang, X.P.; Jia, X.C.; Wang, D.B. Experimental investigation on the solubility of R290 in two mineral oils. *Int. J. Refrig.* **2021**, *124*, 13–19.
35. Lemmon, E.W.; Bell, I.H.; Huber, M.L.; McLinden, M.O. *NIST Standard Reference Database 23: Reference Fluid Thermodynamic and Transport Properties-REFPROP. Version 10.0*; National Institute of Standards and Technology: Gaithersburg, MD, USA, 2019.
36. Bich, W.; Cox, M.G.; Dybkaer, R.; Elster, C.; Estler, W.T.; Hibbert, B.; Imai, H.; Kool, W.; Michotte, C.; Nielsen, L.; et al. Revision of the 'Guide to the Expression of Uncertainty in Measurement'. *Metrologia* **2012**, *49*, 702–705.
37. Fedel, L.; Pernechele, F.; Bobbo, S.; Scattolini, M.; Stryjek, R. Solubility of carbon dioxide in pentaerythritol tetraoctanoate. *Fluid Phase Equilib.* **2009**, *277*, 55–60.
38. Liu, X.Y.; Zheng, Y.; Bai, L.H.; He, M.G. Performance comparison of two absorption-compression hybrid refrigeration systems using R1234yf/ionic liquid as working pair. *Energ. Convers. Manag.* **2019**, *181*, 319–330.
39. Vetere, A. The NRTL equation as a predictive tool for vapor–liquid equilibria. *Fluid Phase Equilib.* **2004**, *218*, 33–39.
40. Pransnitz, J.M.; Lichtenthaler, R.N.; de Azevedo, E.G. *Molecular Thermodynamics of Fluid Phase Equilibria*, 3rd ed.; Prentice Hall PTR: Hoboken, NJ, USA, 1999.
41. Krichevsky, I.R.; Kasarnovsky, J.S. Thermodynamical calculations of solubilities of nitrogen and hydrogen in water at high pressures. *J. Am. Chem. Soc.* **1935**, *57*, 2168–2171.
42. Ji, X.; Adidharma, H. Thermodynamic modeling of CO_2 solubility in ionic liquid with hetero segmented statistical associating fluid theory. *Fluid Phase Equilib.* **2010**, *293*, 141–150.

Disclaimer/Publisher's Note: The statements, opinions and data contained in all publications are solely those of the individual author(s) and contributor(s) and not of MDPI and/or the editor(s). MDPI and/or the editor(s) disclaim responsibility for any injury to people or property resulting from any ideas, methods, instructions or products referred to in the content.